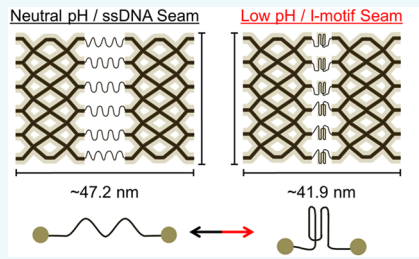


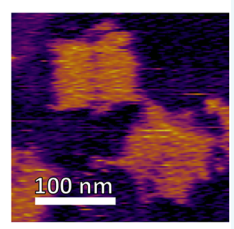
pH-Driven Actuation of DNA Origami via Parallel I-Motif Sequences in Solution and on Surfaces

Jacob M. Majikes, † Lucas C. C. Ferraz, and Thomas H. LaBean*, †

Supporting Information

ABSTRACT: As bottom up DNA nanofabrication creates increasingly complex and dynamic mechanisms, the implementation of actuators within the DNA nanotechnology toolkit has grown increasingly important. One such actuator, the I-motif, is fairly simple in that it consists solely of standard DNA sequences and does not require any modification chemistry or special purification beyond that typical for DNA oligomer synthesis. This study presents a new implementation of parallel I-motif actuators, emphasizing their future potential as drivers of complex internal motion





between substructures. Here we characterize internal motion between DNA origami substructures via AFM and image analysis. Such parallel I-motif design and quantification of actuation provide a useful step toward more complex and effective molecular machines.

he field of molecular robotics seeks to produce artificial nanoscale mechanical systems (armatures, actuators, motors, etc.) capable of performing meaningful work. At this length scale, the viscous forces and low Reynolds number make inertia insignificant compared to random thermal motion. 1 The relative importance of viscosity and thermal motion compared to friction and gravity (which govern macroscale mechanics) results in a significantly different work environment. While engineering in the nanoscale aqueous milieu is relatively new for artificial mechanisms, biological systems consistently and ubiquitously function under these conditions and can act as inspiration for synthetic efforts.

DNA is an ideal nanofabrication material for molecular robotics as its structural properties and assembly code are well understood,³ it is readily and inexpensively synthesized,⁴ and it is commercially available with a wide variety of useful chemical functionalizations. As such, DNA nanotechnology reliably produces structures of arbitrary shape and controllable stiffness that are capable of transferring mechanical force with a relatively straightforward design process. 5–9 Considerable effort has been expended implementing DNA nanotechnology in pursuit of functional molecular robotics with schemes including B–Z helix transitions; 10 strand displacement cascades, 11,12 walkers, tweezers, ¹³ and assembly lines; ¹⁴ multiple DNA origami mechanisms; ^{8,9,15} ion stabilized hairpins; ¹⁶ and pH switched systems. 17-20 The use of pH switched I-motifs is of particular interest as pH is a convenient actuation signal and because the I-motifs are a predictable family of DNA sequences requiring no additional functionalization. 21,22 I-motifs have been used to operate fluorescence quenching cycles; 23 to perform mechanical work, via molecular crowding, on an AFM

cantilever; 20 to lock origami systems; 19 and to drive assembly of dendrimers 24 and gels. 25 This ubiquity makes further implementation of I-motifs useful for operating state switching DNA origami mechanisms, or DOMs. Such DOMs, particularly those consisting of independently functional substructures, are in turn a viable path to molecular robotics.

I-motif sequences consist of C rich ssDNA which folds at low pH into a four-stranded, self-intercalating secondary structure with height proportional to the length of the original ssDNA sequence.²¹ This ssDNA, as any polymer chain, will act as a weak entropic spring whose mean end-to-end distance scales with the length of the polymer, while the I-motif quadruplex is compact and rigid. Since the chain ends can enter and exit from the same side of the quadruplex, the actuation distance can be tuned via the I-motif sequence length. Previous work on I-motif actuators have utilized FRET for monitoring whether the system is in the open or closed state. 17,23,26,27 Here, we are more interested in measurement of large scale motions between substructures for future use in DOMs, rather than on measurement of the individual actuators. Operation of such large DOMs with multiple independent, functional substructures will likely require more than a single I-motif actuator. Parallel I-motifs have been used to lock DNA origami and nanoparticles in place, 28 so the use of I-motifs in parallel between bound substructures (as demonstrated here) is a logical next step. One concern with the use of parallel I-motif actuators bound between substructures is that the transition of

Received: May 22, 2017 Revised: June 11, 2017 Published: June 15, 2017

[†]North Carolina State University, Raleigh, North Carolina 27695, United States

[‡]Universidade Federal do ABC, Santo André 09210-580, Brazil

any one sequence from ssDNA (at neutral pH) into the quadruplex (at low pH) could be inhibited by the other entropic springs. Additionally, change in length is generally more difficult to observe than a binding or locking function. As such, it is of value to create a test system in which to address these concerns

This study presents a DNA actuator consisting of two origami substructures bound by parallel I-motif sequences as a test system for actuation in DOMs. To reduce design overhead and materials expense, the origami actuator was constructed using the recently described mini-M13 scaffold (2.4 kb) instead of the full, wild-type M13 (7.2 kb).²⁹ This had the added benefit of minimizing redesign costs for future design cycles. In performing actuation of these structures on mica surfaces and characterizing their actuation distance via AFM, this study presents an additional step toward the components and techniques required to make true molecular robots capable of performing meaningful work at the nanoscale.

■ RESULTS AND DISCUSSION

The I-motif origami design presented here follows the general staple design pattern and scaffold routing of the Rothemund rectangular origami;⁵ it differed in the use of the mini-M13 scaffold, seam staples modified with I-motif sequences, and excess single-strand scaffold at the seam to accommodate actuation. Seam staples consisted of a 16 base scaffold binding section, a 5 base poly A spacer, and a 21 base I-motif sequence followed by identical spacer and binding sections; the spacer/Imotif sequence was AAA AACC CTA ACC CTA ACC CTA ACC CAA AAA. The mean end-to-end distance per base of ssDNA is approximately 0.66 nm, while the width of an I-motif is \sim 0.8 nm and the length of dsDNA is 0.34 nm/bp. ^{17,30} Using these, we estimated a total origami width of approximately 47.2 nm for the open state (at neutral pH) and approximately 41.9 nm for the closed state (at low pH) as shown in Figure 1. Both width estimates assume the edge staples (red in Figure 1A) are left out of the anneal to prevent blunt-end helix stacking between neighboring origami during imaging.

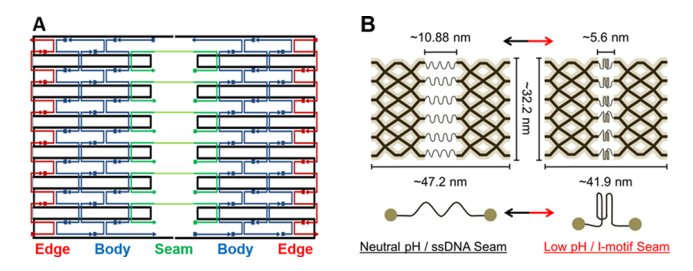


Figure 1. (A) Schematic of scaffold routing and staple placement for I-motif origami: (green) seam staples containing the I-motif sequence; (blue) standard body positions; (red) edge positions omitted from anneals to prevent base stacking. (B) Anticipated dimensions and actuation of I-motif origami.

Figure 2A shows AFM images of samples annealed separately at pH 7.4 and pH 5.4 in sodium cacodylate buffer. The averaged traces, shown in Figure 2B, show a clear difference between the I-motif origami annealed at different pH, with a \sim 2 nm difference in width. This reasonably matches the anticipated actuation, especially given that the anticipated actuation relies on estimated values of ssDNA persistence length to predict the width near neutral pH. ¹⁷ This difference indicates that the I-

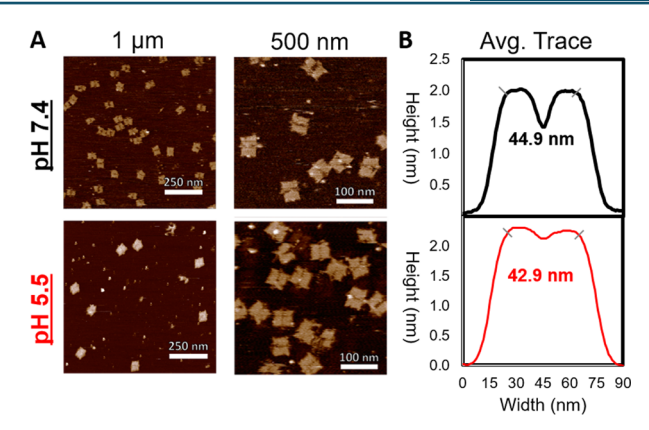


Figure 2. AFM and averaged traces for origami samples annealed at pH 7.4 and pH 5.5: (A) AFM 1 μ m scans (left), 500 nm scans (middle); (B) averaged traces and widths for I-motif origami.

motif sequences are ssDNA at neutral pH and in the quadruplex secondary structure at low pH.

The difference in origami widths when annealed in different buffer conditions indicates that when thermally annealed at a low pH, below the I-motif transition, the origami form and maintain I-motif secondary structure along the seam. It is also worth noting that for the (low) pH 5.5 origami, few origami appear to have an open or skewed (partially open) seam, and those that do also appear to have other damage or annealing defects. The lack of skewed origami indicates that it is rare for a single I-motif sequence, when arranged in parallel with others, to actuate independently of its neighboring strands.

After confirming that origami can be annealed into either open or closed states, in situ actuation of the origami on the mica surface was then tested. The origami, annealed in TAE Mg²⁺ buffer at pH 7.2, were imaged, then actuated on the mica surface into pH 5.5 sodium cacodylate buffer. The sample was imaged again, the surface washing was repeated for pH 7.4 sodium cacodylate, and then the sample was imaged again. The averaged height traces and measured widths for these origami are shown in Figure 3A; actuation between the open and closed states is observed, both in the transition to pH 5.5 and back again to pH 7.4. One difference observed in these results is that origami originally annealed at pH 5.5 show increased height in the bridge/seam region while the surface washed samples do not. It is possible that this difference is related to the ability of I-

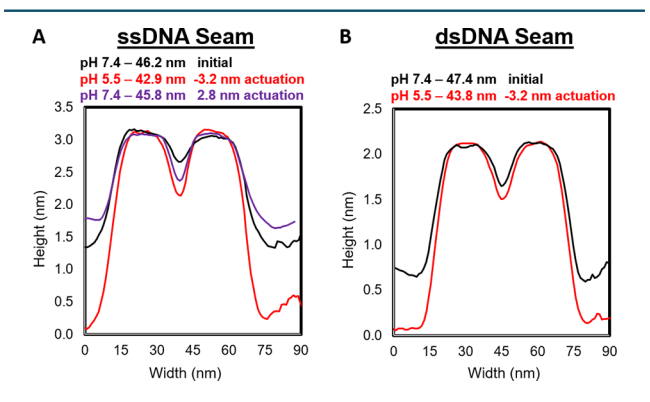


Figure 3. Representative traces for surface wash actuation: (A) annealed in pH 7.4 TAE Mg^{2+} , surface washed to pH 5.5 Na cacodylate, then back to pH 7.4 Na cacodylate; (B) annealed in pH 7.4 TAE Mg buffer with a dsDNA seam, then surface washed to pH 5.5 Na cacodylate.

motif sequences to associate with one another and polymerize. As the I-motif quadruplex can vary its height with its sequence length, it is possible for quadruplexes to form from multiple I-motif sequence strands rather than from the folding of a single strand. Such polymerization would be more likely to occur during the 16 h annealing process in the presence of 10× seam staples than during surface washing. In addition, the narrowness of the seam compared to the radius of curvature of the AFM tip discourages one from drawing too many conclusions based purely on the measured seam width/height.

As the weak entropic spring of ssDNA may not be an optimal open state, the previous experiment was repeated in which the open state was dsDNA rather than ssDNA. For this test, the origami were annealed with an additional ssDNA strand complementary to the I-motif sequence. This sequence contained multiple mismatches to lower the melting temperature of the dsDNA and to prevent G-quadruplex formation on the complementary strand. Figure 3B shows that the initial, neutral pH trace (black) still has a visible trough along the seam, which we anticipated would be reduced due to dsDNA along the seam. That the initial, neutral pH, width of the dsDNA seamed origami is slightly longer than its low pH counterpart indicates that the mean end-to-end distance used in our initial estimates is not perfectly applicable to this system. This is unsurprising as the value used for this mean end-to-end distance as a function of ssDNA length was obtained from experimental studies in which the ssDNA was unbound and free on both sides.³⁰ These observations indicate that the actuation of parallel I-motifs is relatively robust and may be implemented to drive internal motion in more complex systems.

CONCLUSIONS

This work expands on previous work describing switching of the same structure by an applied electric field on highly oriented pyrolytic graphene (HOPG). ³¹ The present paper also provides a more detailed description of the origami design, quantification of actuation distance, and pH driven actuation. We expect that integration of large numbers of parallel I-motifs, or other actuators, in combination with topologically complex origami could create DOMs capable of driving work at the nanoscale.

In conclusion, we have demonstrated that multiple I-motif domains, working in parallel, can perform actuation and reversibly control internal motions of DNA nanostructures. We have also shown that this, and other similar actuations, can be monitored via AFM imaging, which could be potentially useful for DOMs consisting of multiple substructures where the use of FRET pairs may prove insufficient. Future work on such analysis would include automation of trace alignment and calculation of statistical confidence for actuation width.

METHODS

The origami samples were annealed in 30 μ L aliquots at 25 nM mini-M13 scaffold and 250 nM staple concentration in buffer containing 12.5 mM MgCl₂. Buffers consisted of either TAE (40 mM Tris acetate, 1 mM EDTA at pH 7.2) or sodium cacodylate (50 mM cacodylate, 1 mM EDTA at pH 7.4 or 5.5). The 25 nM scaffold concentration was chosen as the mini-M13 scaffold is one-third the size of standard M13; an anneal containing 25 nM mini-M13 will have a similar total nucleobase concentration to a 7.5 nM M13 scaffold anneal. Sodium

cacodylate buffer was used during the annealing of some samples as it holds pH constant across wider temperature ranges than tris buffer. Given that TAE is less toxic and more commonly used for origami annealing protocols, it was used as the initial buffer for samples actuated via surface wash. Anneals were performed in a thermocycler with a linear ramp from 90 to 25 $^{\circ}\text{C}$ over 16 h. All buffers used in annealing and imaging were autoclaved prior to use.

Imaging was performed with an Asylum Cypher AFM in liquid tapping mode using Biolever-Mini probes (Olympus BL-AC40TS). Origami were imaged on mica pucks which were freshly cleaved before addition of sample/buffer. The samples were diluted to ~0.45 nM scaffold/origami concentration before pipetting onto the mica surface.

As the anticipated actuation distance, \sim 5 nm, is less than the \sim 8 nm tip radius of the AFM probes, determination of average origami width required multistep analysis of AFM images. This process is outlined in Figure 4. For each of at least 30 origami

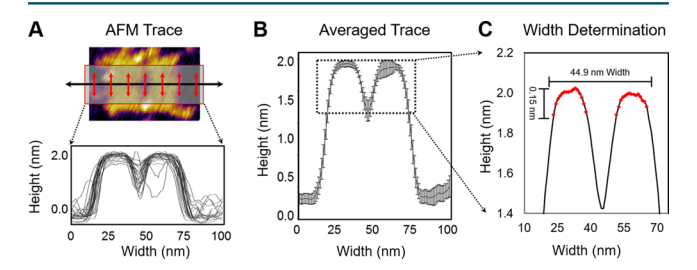


Figure 4. (A) AFM trace for single origami averaging height over a 25 nm width perpendicular to the trace line and 30 AFM traces aligned about origami seam. (B) Averaged trace with STDV error bars. (C) Height thresholding of the origami crown to determine width.

in each sample, height traces were measured across the origami width as shown in Figure 4A. If the trace is taken only as the measured height along pixels under the black line in Figure 4A, the height measurements have a great deal of variability due to the intersection of the black trace line with the crosshatched dsDNA helices of the origami. This is a barrier to measuring consistent widths for each origami. As such, each point in the height trace was set as the average of the points above and below it perpendicular to the trace line. In Figure 4A this is shown as a red box with a 25 nm width, centered on the trace line. As shown in the lower half of Figure 1C, this results in consistent height traces for individual origami. For each sample at least 30 such height traces were aligned by sight along the seam. These traces were then averaged, as shown in Figure 1D.

After obtaining the average height trace for each sample of origami, their width was determined. One complication in this regard was that the neutral and low pH samples consistently gave different height measurements. As AFM images are convolutions of the tip and sample, this height difference would result in an artificially higher width for the taller samples if the full width at half-maximum was used. Instead, the width of the origami "crown" was defined and calculated. The height of the origami crown was calculated from the average of the highest 10 points in the height trace. All points on the trace with a height within 0.15 nm of the crown height were plotted, shown in Figure 4C. This height range is discussed in detail in the Supporting Information section S1. This 0.15 nm height was chosen as it is approximately the height between the "top" of the crown and the curvature occurring before the origami edge. The width was then defined as the distance between the

furthest of these points. This larger distance was used because the substructure actuation, rather than that of just the actuators, is likely to be the figure of merit in more complex systems with numerous motions and substructures. The results reported here were robust and fairly insensitive to small changes in the definition of the crown.

Samples for surface washing were annealed in the standard TAE $\mathrm{Mg^{2+}}$ buffer at pH 7.2. After the samples were imaged, surface washing was performed by unmounting the AFM probe and pipetting/replacing the buffer droplet with 45 μ L of the destination buffer at the desired pH, supplemented with 100 mM NaCl, a minimum of 3 times. NaCl was used as monovalent cations have been shown to allow diffusion of origami across mica surfaces. The sample was then incubated for 5 min and the buffer was washed another 3 times into destination buffer containing only $\mathrm{Mg^{2+}}$ and not $\mathrm{Na^{+}}$. This rebound the origami to the mica surface. The AFM tip was then rinsed with DI water, dried, wetted with 30 μ L of destination buffer, and the sample was then reimaged.

■ ASSOCIATED CONTENT

S Supporting Information

The Supporting Information is available free of charge on the ACS Publications website at DOI: 10.1021/acs.bioconjchem.7b00288.

AFM images and individual origami traces for all samples (PDF)

AUTHOR INFORMATION

Corresponding Author

*E-mail: thlabean@ncsu.edu.

ORCID

Jacob M. Majikes: 0000-0003-3177-4941 Thomas H. LaBean: 0000-0002-6739-2059

Notes

The authors declare no competing financial interest.

ACKNOWLEDGMENTS

We acknowledge CAPES and CNPq for a Science without Borders Scholarship which permitted L.C.C.F. to collaborate on this project. We also acknowledge funding from the U.S. National Science Foundation (Grants ECCS-EPMD-1231888, ECCS-EPMD-1608847, OISE-IRES-1559077, and CBET-BME-1603179).

ABBREVIATIONS

DNA, deoxyribonucleic acid; AFM, atomic force microscopy; DOM, DNA origami mechanism

REFERENCES

- (1) Kay, E. R., Leigh, D. a., and Zerbetto, F. (2007) Synthetic molecular motors and mechanical machines. *Angew. Chem., Int. Ed.* 46, 72–191.
- (2) Hagiya, M., Konagaya, A., Kobayashi, S., Saito, H., and Murata, S. (2014) Molecular robots with sensors and intelligence. *Acc. Chem. Res.* 47, 1681–1690.
- (3) Pedersen, R., Marchi, A. N., Majikes, J. M., Nash, J. A., Estrich, N. A., Courson, D. S., Hall, C. K., Craig, S. L., and LaBean, T. H. (2015) Properties of DNA. In *Handbook of Nanomaterials Properties* pp 1125—1157, Springer, Berlin, DOI: 10.1007/978-3-642-31107-9 10.
- (4) Carlson, R. (2009) The changing economics of DNA synthesis. *Nat. Biotechnol.* 27, 1091–4.
- (5) Rothemund, P. W. K. (2006) Folding DNA to create nanoscale shapes and patterns. *Nature 440*, 297–302.
- (6) Rothemund, P. W. K. (2005) Design of DNA origami. In Proceedings of the 2005 IEEE/ACM International Conference on Computer-Aided Design pp 470-477, IEEE Computer Society, Washington, DC.
- (7) Zhou, L., Marras, A. E., Su, H. J., and Castro, C. E. (2014) DNA origami compliant nanostructures with tunable mechanical properties. *ACS Nano* 8, 27–34.
- (8) Zhou, L., Marras, A. E., Castro, C. E., and Su, H.-J. (2016) Pseudorigid-Body Models of Compliant DNA Origami Mechanisms. *J. Mech. Robot.* 8, 51013.
- (9) Marras, A. E., Zhou, L., Su, H.-J., and Castro, C. E. (2015) Programmable motion of DNA origami mechanisms TL 112. *Proc. Natl. Acad. Sci. U. S. A. 112*, 713–718.
- (10) Mao, C., Sun, W., Shen, Z., and Seeman, N. C. (1999) A nanomechanical device based on the B-Z transition of DNA. *Nature* 397, 144–146.
- (11) Mavroidis, C., and Ferreira, A. (2013) Nanorobotics: Current Approaches and Techniques pp 1-467, Vol. 382.
- (12) Bath, J., and Turberfield, A. J. (2007) DNA nanomachines. *Nat. Nanotechnol.* 2, 275–284.
- (13) Zhang, D. Y., and Seelig, G. (2011) Dynamic DNA nanotechnology using strand- displacement reactions. *Nat. Chem.* 3, 103–113.
- (14) Gu, H., Chao, J., Xiao, S.-J., and Seeman, N. C. (2010) A proximity-based programmable DNA nanoscale assembly line. *Nature* 465, 202–5.
- (15) Marras, A. E., Zhou, L., Kolliopoulos, V., Su, H.-J., and Castro, C. E. (2016) Directing folding pathways for multi-component DNA origami nanostructures with complex topology. *New J. Phys.* 18, 055005.
- (16) Porchetta, A., Vallée-Bélisle, A., Plaxco, K. W., and Ricci, F. (2013) Allosterically tunable, DNA-based switches triggered by heavy metals. *J. Am. Chem. Soc.* 135, 13238–13241.
- (17) Liu, D., and Balasubramanian, S. (2003) A Proton-Fuelled DNA Nanomachine. *Angew. Chem., Int. Ed.* 42, 5734–5736.
- (18) Seela, F., and Budow, S. (2006) pH-Dependent Assembly of DNA-Gold Nanoparticles Based on the i-Motif: A Switchable Device with the Potential of a Nanomachine. *Helv. Chim. Acta* 89, 1978–1985.
- (19) Wu, N., and Willner, I. (2016) PH-Stimulated Reconfiguration and Structural Isomerization of Origami Dimer and Trimer Systems. *Nano Lett.* 16, 6650–6655.
- (20) Eom, K., Jung, H., Lee, G., Park, J., Nam, K., Lee, S. W., Yoon, D. S., Yang, J., and Kwon, T. (2012) Nanomechanical actuation driven by light-induced DNA fuel. *Chem. Commun. (Cambridge, U. K.)* 48, 955–7
- (21) Yatsunyk, L. a., Mendoza, O., and Mergny, J. L. (2014) "Nano-oddities": Unusual nucleic acid assemblies for DNA-based nanostructures and nanodevices. *Acc. Chem. Res.* 47, 1836–1844.
- (22) Dong, Y., Yang, Z., and Liu, D. (2014) DNA nanotechnology based on i-motif structures. Acc. Chem. Res. 47, 1853–1860.
- (23) Liu, D., and Balasubramanian, S. (2003) A proton-fuelled DNA nanomachine. *Angew. Chem., Int. Ed.* 42, 5734–6.

(24) Zhou, T., Chen, P., Niu, L., Jin, J., Liang, D., Li, Z., Yang, Z., and Liu, D. (2012) pH-responsive size-tunable self-assembled DNA dendrimers. *Angew. Chem., Int. Ed.* 51, 11271–4.

- (25) Cheng, E., Xing, Y., Chen, P., Yang, Sun, Y., Zhou, D., Xu, T., Fan, Q., and Liu, D. (2009) A pH-triggered, fast-responding DNA hydrogel. *Angew. Chem., Int. Ed.* 48, 7660–7663.
- (26) Surana, S., Bhat, J. M., Koushika, S. P., and Krishnan, Y. (2011) An autonomous DNA nanomachine maps spatiotemporal pH changes in a multicellular living organism. *Nat. Commun.* 2, 340.
- (27) Day, H. A., Huguin, C., and Waller, A. E. (2013) Silver cations fold i-motif at neutral pH. Chem. Commun. 49, 7696-7698.
- (28) Wang, W., Liu, H., Liu, D., Xu, Y., Yang, Y., and Zhou, D. (2007) Use of the interparticle i-motif for the controlled assembly of gold nanoparticles. *Langmuir* 23, 11956–11959.
- (29) Brown, S., Majikes, J., Martinez, A., Giron, T. M., Fennell, H., Samano, E. C., and LaBean, T. H. (2015) An easy-to-prepare miniscaffold for DNA origami. *Nanoscale* 7, 16621–16624.
- (30) Murphy, M. C., Rasnik, I., Cheng, W., Lohman, T. M., and Ha, T. (2004) Probing single-stranded DNA conformational flexibility using fluorescence spectroscopy. *Biophys. J.* 86, 2530–7.
- (31) Campos, R., Zhang, S., Majikes, J. M., Ferraz, L. C. C., LaBean, T. H., Dong, M. D., and Ferapontova, E. E. (2015) Electronically addressable nanomechanical switching of i-motif DNA origami assembled on basal plane HOPG. *Chem. Commun.* 51, 14111–14114.
- (32) Woo, S., and Rothemund, P. W. K. (2014) Self-assembly of two-dimensional DNA origami lattices using cation-controlled surface diffusion. *Nat. Commun.* 5, 4889.